

# Mass spectra and Regge trajectories of light mesons in the relativistic quark model

D. Ebert<sup>1</sup>, R. N. Faustov<sup>2</sup> and V. O. Galkin<sup>2</sup>

<sup>1</sup> *Institut für Physik, Humboldt-Universität zu Berlin,  
Newtonstr. 15, D-12489 Berlin, Germany*

<sup>2</sup> *Dorodnicyn Computing Centre, Russian Academy of Sciences,  
Vavilov Str. 40, 119991 Moscow, Russia*

Masses of the ground, orbitally and radially excited states of quark-antiquark mesons composed from the light ( $u, d, s$ ) quarks are calculated within the framework of the relativistic quark model based on the quasipotential approach. The relativistic treatment of the light quark dynamics results in mass spectra which agree well with available experimental data for the masses of the most well-established states. The Regge trajectories for angular and radial excitations are constructed, and their linearity, parallelism and equidistance are verified. The assignment of experimentally observed light mesons to particular Regge trajectories is based on their masses and quantum numbers.

PACS numbers: 14.40.Aq, 14.40.Cs, 14.40.Ev, 12.39.Ki

## I. INTRODUCTION

Last years an extensive analysis of the data on highly excited light non-strange meson states up to a mass of 2400 MeV collected by the Crystal Barrel experiment at LEAR (CERN) has been published [1, 2]. The classification of these new data requires a better theoretical understanding of light meson mass spectra. The aim of this paper is to apply the relativistic quark model which proved to be successful in studying various properties of heavy hadrons to the calculation of the masses of the radially and orbitally excited light meson states. All main assumptions and fixed values of model parameters are preserved in the present investigation. Light quarks are treated fully relativistically without the  $v/c$  expansion. Various non-strange and strange meson states with masses up to 2500 MeV are considered. This is especially important, since light exotic states (such as tetraquarks, glueballs, hybrids) predicted by quantum chromodynamics (QCD) are expected to have masses in this range [3, 4, 5, 6]. The experimental data show that a large degeneracy emerges in the spectra of the orbitally and radially excited resonances. It is argued [7] that the states of the same spin with different isospins and opposite parities are approximately degenerate in the interval 1700-2400 MeV. An intensive debate is going on now in the literature whether the chiral symmetry is restored for highly excited states (see e.g. [7, 8] and references therein). Various phenomenological and theoretical arguments, such as quasiclassical considerations, AdS/QCD etc. are used.

A vast literature on the light meson spectroscopy is available. Different attempts to study light mesons on the basis of the relativized quark model [9], the Dyson-Schwinger and Bethe-Salpeter equations [10, 11, 12], the Tamm-Dancoff method [13], chiral quark models

with spontaneous symmetry breaking like the Nambu-Jona-Lasinio model [14], finite-energy sum rules in QCD [15], lattice QCD [16], AdS/QCD models [17, 18], etc. were undertaken. Therefore we mostly refer to the recent reviews where the references to earlier review and original papers can be found.

In Refs. [19, 20] we studied the masses of ground and radially excited states of light mesons on the basis of the three-dimensional relativistic wave equation with the QCD-motivated potential. In this analysis we took into account the highly relativistic dynamics of light quarks and carried out all calculations without either the  $v/c$  or  $1/m_q$  expansions. We also used the expression for the QCD coupling constant  $\alpha_s$  which exhibits freezing at small values of the momentum transfer. Good overall agreement of the obtained predictions and experimental data was found. The consistent relativistic treatment of the light quark dynamics resulted in a nonlinear dependence of the bound state equation on the meson mass which allowed to get the correct values of the pion and kaon masses in the model with the explicitly broken chiral symmetry. The obtained wave functions of the pion and kaon were successfully applied for the relativistic calculation of their decay constants and electromagnetic form factors [20]. Recently, in the framework of the same approach we calculated masses of the ground-state light tetraquarks using the diquark-antidiquark picture [21]. It was found that scalar mesons with masses below 1 GeV agree well with the light-tetraquark interpretation. Indeed, it explains naturally the peculiar inverted pattern of the mass ordering of the lightest scalar flavour  $SU(3)$  nonet. Here we investigate the Regge trajectories both in  $(M^2, J)$  and  $(M^2, n_r)$  planes ( $M$  is the mass,  $J$  is the spin and  $n_r$  is the radial quantum number of the meson state), check their linearity and equidistance which follow from experimental data [22]. The assignment of experimentally observed mesons to particular Regge trajectories is proposed.

The paper is organized as follows. In Section II we describe the relativistic quark model, giving its main assumptions and parameters which were fixed in previous considerations. The relativistic quasipotential of the light quark-antiquark interaction in the meson is constructed in Sec III. The procedure which makes this potential local and avoids the arising fictitious singularities is described in detail. In Sec. IV the obtained results for the masses of orbital and radial excitations of light mesons are presented and compared with available experimental data. Finally, the Regge trajectories are constructed. Their linearity, parallelism and equidistance is verified, and the slopes of different trajectories are compared. Section V contains our conclusions.

## II. RELATIVISTIC QUARK MODEL

In the relativistic quark model based on the quasipotential approach a meson is described by the wave function of the bound quark-antiquark state, which satisfies the quasipotential equation of the Schrödinger type [23]

$$\left( \frac{b^2(M)}{2\mu_R} - \frac{\mathbf{p}^2}{2\mu_R} \right) \Psi_M(\mathbf{p}) = \int \frac{d^3q}{(2\pi)^3} V(\mathbf{p}, \mathbf{q}; M) \Psi_M(\mathbf{q}), \quad (1)$$

where the relativistic reduced mass is

$$\mu_R = \frac{E_1 E_2}{E_1 + E_2} = \frac{M^4 - (m_1^2 - m_2^2)^2}{4M^3}, \quad (2)$$

and  $E_1, E_2$  are given by

$$E_1 = \frac{M^2 - m_2^2 + m_1^2}{2M}, \quad E_2 = \frac{M^2 - m_1^2 + m_2^2}{2M}. \quad (3)$$

Here  $M = E_1 + E_2$  is the meson mass,  $m_{1,2}$  are the quark masses, and  $\mathbf{p}$  is their relative momentum. In the center-of-mass system the relative momentum squared on mass shell reads

$$b^2(M) = \frac{[M^2 - (m_1 + m_2)^2][M^2 - (m_1 - m_2)^2]}{4M^2}. \quad (4)$$

The kernel  $V(\mathbf{p}, \mathbf{q}; M)$  in Eq. (1) is the quasipotential operator of the quark-antiquark interaction. It is constructed with the help of the off-mass-shell scattering amplitude, projected onto the positive energy states. Constructing the quasipotential of the quark-antiquark interaction, we have assumed that the effective interaction is the sum of the usual one-gluon exchange term with the mixture of long-range vector and scalar linear confining potentials, where the vector confining potential contains the Pauli interaction. The quasipotential is then defined by

$$V(\mathbf{p}, \mathbf{q}; M) = \bar{u}_1(p)\bar{u}_2(-p)\mathcal{V}(\mathbf{p}, \mathbf{q}; M)u_1(q)u_2(-q), \quad (5)$$

with

$$\mathcal{V}(\mathbf{p}, \mathbf{q}; M) = \frac{4}{3}\alpha_s D_{\mu\nu}(\mathbf{k})\gamma_1^\mu\gamma_2^\nu + V_{\text{conf}}^V(\mathbf{k})\Gamma_1^\mu\Gamma_{2;\mu} + V_{\text{conf}}^S(\mathbf{k}),$$

where  $\alpha_s$  is the QCD coupling constant,  $D_{\mu\nu}$  is the gluon propagator in the Coulomb gauge

$$D^{00}(\mathbf{k}) = -\frac{4\pi}{\mathbf{k}^2}, \quad D^{ij}(\mathbf{k}) = -\frac{4\pi}{k^2} \left( \delta^{ij} - \frac{k^i k^j}{\mathbf{k}^2} \right), \quad D^{0i} = D^{i0} = 0, \quad (6)$$

and  $\mathbf{k} = \mathbf{p} - \mathbf{q}$ ;  $\gamma_\mu$  and  $u(p)$  are the Dirac matrices and spinors

$$u^\lambda(p) = \sqrt{\frac{\epsilon(p) + m}{2\epsilon(p)}} \left( \frac{1}{\epsilon(p) + m} \begin{pmatrix} 1 \\ \boldsymbol{\sigma}\mathbf{p} \end{pmatrix} \right) \chi^\lambda, \quad (7)$$

with  $\epsilon(p) = \sqrt{p^2 + m^2}$ . The effective long-range vector vertex is given by

$$\Gamma_\mu(\mathbf{k}) = \gamma_\mu + \frac{i\kappa}{2m}\sigma_{\mu\nu}k^\nu, \quad (8)$$

where  $\kappa$  is the Pauli interaction constant characterizing the anomalous chromomagnetic moment of quarks. Vector and scalar confining potentials in the nonrelativistic limit reduce to

$$\begin{aligned} V_{\text{conf}}^V(r) &= (1 - \varepsilon)(Ar + B), \\ V_{\text{conf}}^S(r) &= \varepsilon(Ar + B), \end{aligned} \quad (9)$$

reproducing

$$V_{\text{conf}}(r) = V_{\text{conf}}^S(r) + V_{\text{conf}}^V(r) = Ar + B, \quad (10)$$

where  $\varepsilon$  is the mixing coefficient.

All the model parameters have the same values as in our previous papers [23, 24]. The light constituent quark masses  $m_u = m_d = 0.33$  GeV,  $m_s = 0.5$  GeV and the parameters

of the linear potential  $A = 0.18 \text{ GeV}^2$  and  $B = -0.3 \text{ GeV}$  have the usual values of quark models. The value of the mixing coefficient of vector and scalar confining potentials  $\varepsilon = -1$  has been determined from the consideration of charmonium radiative decays [23]. Finally, the universal Pauli interaction constant  $\kappa = -1$  has been fixed from the analysis of the fine splitting of heavy quarkonia  $^3P_J$ - states [23]. In this case, the long-range chromomagnetic interaction of quarks, which is proportional to  $(1 + \kappa)$ , vanishes in accordance with the flux-tube model.

### III. QUASIPOTENTIAL OF THE LIGHT QUARK-ANTIQUARK INTERACTION

The quasipotential (5) can be used for arbitrary quark masses. The substitution of the Dirac spinors (7) into (5) results in an extremely nonlocal potential in the configuration space. Clearly, it is very hard to deal with such potentials without any additional transformations. In order to simplify the relativistic  $q\bar{q}$  potential, we make the following replacement in the Dirac spinors:

$$\epsilon_{1,2}(p) = \sqrt{m_{1,2}^2 + \mathbf{p}^2} \rightarrow E_{1,2} \quad (11)$$

(see the discussion of this point in [19, 24]). This substitution makes the Fourier transformation of the potential (5) local. Calculating the potential, we keep only operators quadratic in the momentum acting on  $V_{\text{Coul}}$ ,  $V_{\text{conf}}^{V,S}$  and replace  $\mathbf{p}^2 \rightarrow E_{1,2}^2 - m_{1,2}^2$  in higher order operators in accord with Eq. (11) preserving the symmetry under the  $(1 \leftrightarrow 2)$  exchange. It is necessary to point out that such substitutions lead to the quark-antiquark potential which commutes with operators of the total angular momentum and the orbital angular momentum. Therefore  $J$  and  $L$  are good quantum numbers, as in the nonrelativistic approach. However the nonlinear dependence of the interaction potential on the meson mass effectively takes into account the relativistic character of the light quark interaction. Note that the global features of highly excited light mesons can be well understood in terms of the relativistic relations involving  $J$  as well as nonrelativistic relations involving  $L$  [17, 25].

The substitution (11) works well for the confining part of the potential. However, it leads to fictitious singularities  $1/r^3$  and  $\delta^3(\mathbf{r})$  at the origin arising from the one-gluon exchange part ( $\Delta V_{\text{Coul}}(r)$ ), which is absent in the initial potential. Note that these singularities are not important if they are treated perturbatively. Since we are not using the expansion in  $v/c$  and are solving the quasipotential equation with the complete relativistic potential, an additional analysis is required. Such singular contributions emerge, e.g., from the following terms

$$\frac{\mathbf{k}^2}{[\epsilon_i(q)(\epsilon_i(q) + m_i)\epsilon_i(p)(\epsilon_i(p) + m_i)]^{1/2}} V_{\text{Coul}}(\mathbf{k}^2),$$

$$\frac{\mathbf{k}^2}{[\epsilon_1(q)\epsilon_1(p)\epsilon_2(q)\epsilon_2(p)]^{1/2}} V_{\text{Coul}}(\mathbf{k}^2), \quad (12)$$

if we simply replace  $\epsilon_{1,2} \rightarrow E_{1,2}$ . However, the Fourier transforms of expressions (12) are less singular at  $r \rightarrow 0$ . To avoid such fictitious singularities we note that if the binding effects are taken into account, it is necessary to replace  $\epsilon_{1,2} \rightarrow E_{1,2} - \eta_{1,2}V$ , where  $V$  is the quark interaction potential and  $\eta_{1,2} = m_{2,1}/(m_1 + m_2)$ . At small distances  $r \rightarrow 0$ , the Coulomb singularity in  $V$  dominates and gives the correct asymptotic behaviour. Therefore, we replace  $\epsilon_{1,2} \rightarrow E_{1,2} - \eta_{1,2}V_{\text{Coul}}$  in the Fourier transforms of terms (12) (cf. [26]). We

used a similar regularization of singularities in the analysis of heavy-light meson spectra [24]. Finally, we ignore the annihilation terms in the quark potential since they contribute only in the isoscalar channels and are suppressed in the  $s\bar{s}$  vector channel.

The resulting  $q\bar{q}$  potential then reads

$$V(r) = V_{\text{SI}}(r) + V_{\text{SD}}(r), \quad (13)$$

where the spin-independent potential has the form

$$\begin{aligned} V_{\text{SI}}(r) = & V_{\text{Coul}}(r) + V_{\text{conf}}(r) + \frac{(E_1^2 - m_1^2 + E_2^2 - m_2^2)^2}{4(E_1 + m_1)(E_2 + m_2)} \left\{ \frac{1}{E_1 E_2} V_{\text{Coul}}(r) \right. \\ & + \frac{1}{m_1 m_2} \left( 1 + (1 + \kappa) \left[ (1 + \kappa) \frac{(E_1 + m_1)(E_2 + m_2)}{E_1 E_2} \right. \right. \\ & \left. \left. - \left( \frac{E_1 + m_1}{E_1} + \frac{E_1 + m_2}{E_2} \right) \right] \right) V_{\text{conf}}^V(r) + \frac{1}{m_1 m_2} V_{\text{conf}}^S(r) \left. \right\} \\ & + \frac{1}{4} \left( \frac{1}{E_1(E_1 + m_1)} \Delta \tilde{V}_{\text{Coul}}^{(1)}(r) + \frac{1}{E_2(E_2 + m_2)} \Delta \tilde{V}_{\text{Coul}}^{(2)}(r) \right) \\ & - \frac{1}{4} \left[ \frac{1}{m_1(E_1 + m_1)} + \frac{1}{m_2(E_2 + m_2)} - (1 + \kappa) \left( \frac{1}{E_1 m_1} + \frac{1}{E_2 m_2} \right) \right] \Delta V_{\text{conf}}^V(r) \\ & + \frac{(E_1^2 - m_1^2 + E_2^2 - m_2^2)}{8m_1 m_2 (E_1 + m_1)(E_2 + m_2)} \Delta V_{\text{conf}}^S(r) + \frac{1}{E_1 E_2} \frac{\mathbf{L}^2}{2r} \bar{V}'_{\text{Coul}}(r), \end{aligned} \quad (14)$$

and the spin-dependent potential is given by

$$V_{\text{SD}}(r) = a_1 \mathbf{L}\mathbf{S}_1 + a_2 \mathbf{L}\mathbf{S}_2 + b \left[ -\mathbf{S}_1\mathbf{S}_2 + \frac{3}{r^2} (\mathbf{S}_1\mathbf{r})(\mathbf{S}_2\mathbf{r}) \right] + c \mathbf{S}_1\mathbf{S}_2 + d (\mathbf{L}\mathbf{S}_1)(\mathbf{L}\mathbf{S}_2), \quad (15)$$

$$\begin{aligned} a_1 = & \frac{1}{2E_1 E_2} \left\{ \left( 2 + \frac{2m_2}{E_1 + m_1} \right) \frac{1}{r} \bar{V}'_{\text{Coul}}(r) - \frac{2E_2}{E_1 + m_1} \frac{1}{r} V'_{\text{conf}}(r) - \left( 1 + \frac{2m_2}{E_1 + m_1} \right) \right. \\ & \times \left( \frac{E_1 - m_1}{2m_1} - (1 + \kappa) \frac{E_1 + m_1}{2m_1} \right) \frac{2}{r} V_{\text{conf}}^V(r) + \left( \frac{E_1 - m_1}{E_2 + m_2} + \frac{E_2 - m_2}{E_1 + m_1} \right) \frac{1}{r} V_{\text{conf}}^V(r) \left. \right\} \\ & + \frac{1}{4E_1 E_2 (E_1 + m_1)(E_2 + m_2)} \left[ \frac{1}{r} \hat{V}_{\text{Coul}}^{\text{III}}(r) + \frac{1}{r} V_{\text{conf}}^{\text{III}S}(r) + \left( \frac{E_1}{m_1} - 2(1 + \kappa) \frac{E_1 + m_1}{2m_1} \right) \right. \\ & \left. \times \left( \frac{E_2}{m_2} - 2(1 + \kappa) \frac{E_2 + m_2}{2m_2} \right) \frac{1}{r} V_{\text{conf}}^{\text{III}V}(r) \right], \end{aligned} \quad (16)$$

$$a_2 = a_1(1 \leftrightarrow 2), \quad (17)$$

$$\begin{aligned} b = & \frac{1}{3E_1 E_2} \left[ \frac{1}{r} \bar{V}'_{\text{Coul}}(r) - \bar{V}''_{\text{Coul}}(r) + \left( \frac{E_1 - m_1}{2m_1} - (1 + \kappa) \frac{E_1 + m_1}{2m_1} \right) \right. \\ & \left. \times \left( \frac{E_2 - m_2}{2m_2} - (1 + \kappa) \frac{E_2 + m_2}{2m_2} \right) \left( \frac{1}{r} V_{\text{conf}}^V(r) - V_{\text{conf}}^{\text{II}V}(r) \right) \right], \end{aligned} \quad (18)$$

$$\begin{aligned} c = & \frac{2}{3E_1 E_2} \left[ \Delta \bar{V}_{\text{Coul}}(r) + \left( \frac{E_1 - m_1}{2m_1} - (1 + \kappa) \frac{E_1 + m_1}{2m_1} \right) \right. \\ & \left. \times \left( \frac{E_2 - m_2}{2m_2} - (1 + \kappa) \frac{E_2 + m_2}{2m_2} \right) \Delta V_{\text{conf}}^V(r) \right] \end{aligned} \quad (19)$$

$$d = -\frac{1}{E_1 E_2 (E_1 + m_1)(E_2 + m_2)} \frac{1}{r^2} \left[ \hat{V}'_{\text{Coul}}(r) - \hat{V}''_{\text{Coul}}(r) + \frac{1}{r} \hat{V}'_{\text{conf}}(r) - \hat{V}''_{\text{conf}}(r) \right], \quad (20)$$

with

$$\begin{aligned}
V_{\text{Coul}}(r) &= -\frac{4}{3} \frac{\alpha_s}{r}, \\
\tilde{V}_{\text{Coul}}^{(i)}(r) &= V_{\text{Coul}}(r) \frac{1}{\left(1 + \eta_i \frac{4}{3} \frac{\alpha_s}{E_i} \frac{1}{r}\right) \left(1 + \eta_i \frac{4}{3} \frac{\alpha_s}{E_i + m_i} \frac{1}{r}\right)}, \quad (i = 1, 2), \\
\bar{V}_{\text{Coul}}(r) &= V_{\text{Coul}}(r) \frac{1}{\left(1 + \eta_1 \frac{4}{3} \frac{\alpha_s}{E_1} \frac{1}{r}\right) \left(1 + \eta_2 \frac{4}{3} \frac{\alpha_s}{E_2} \frac{1}{r}\right)}, \quad \eta_{1,2} = \frac{m_{2,1}}{m_1 + m_2}, \\
\hat{V}(r) &= \frac{V(r)}{\left(1 + \eta_1 \frac{4}{3} \frac{\alpha_s}{E_1} \frac{1}{r}\right) \left(1 + \eta_1 \frac{4}{3} \frac{\alpha_s}{E_1 + m_1} \frac{1}{r}\right) \left(1 + \eta_2 \frac{4}{3} \frac{\alpha_s}{E_2} \frac{1}{r}\right) \left(1 + \eta_2 \frac{4}{3} \frac{\alpha_s}{E_2 + m_2} \frac{1}{r}\right)}. \quad (21)
\end{aligned}$$

Here we put  $\alpha_s \equiv \alpha_s(\mu_{12}^2)$  with  $\mu_{12} = 2m_1 m_2 / (m_1 + m_2)$ . We adopt for  $\alpha_s(\mu^2)$  the simplest model with freezing [27], namely

$$\alpha_s(\mu^2) = \frac{4\pi}{\beta_0 \ln \frac{\mu^2 + M_B^2}{\Lambda^2}}, \quad \beta_0 = 11 - \frac{2}{3} n_f, \quad (22)$$

where the background mass is  $M_B = 2.24\sqrt{A} = 0.95$  GeV [27], and  $\Lambda = 413$  MeV was fixed from fitting the  $\rho$  mass.<sup>1</sup> We put the number of flavours  $n_f = 2$  for  $\pi$ ,  $\rho$ ,  $K$ ,  $K^*$  and  $n_f = 3$  for  $\phi$ . As a result we obtain  $\alpha_s(\mu_{ud}^2) = 0.730$ ,  $\alpha_s(\mu_{us}^2) = 0.711$  and  $\alpha_s(\mu_{ss}^2) = 0.731$ . Note that the other popular parametrisation of  $\alpha_s$  with freezing [28] gives close values.

#### IV. RESULTS AND DISCUSSION

The calculated masses of light unflavoured and strange mesons are given in Tables I and II. They are confronted with available experimental data from PDG Particle Listings including data from the ‘‘Further States’’ Section [29]. We find good agreement of our predictions with data. Most of the well-established state masses are reproduced in our model.

We do not consider the mixing of states in the isoscalar sector. Therefore the predictions in Table I are given for the pure  $q\bar{q}$  and  $s\bar{s}$  states. Such mixing is mostly important in the pseudoscalar sector. We follow the  $\eta - \eta'$  mixing scheme proposed in Ref. [30] and take the phenomenological values of the mixing angle  $\phi = 38^\circ$  and the decay constant ratio  $y \equiv f_q/f_s = 0.81$ . Using our values for the mass of  $M_{\eta_{s\bar{s}}}$  and the pion mass we get  $M_\eta = 573$  MeV and  $M_{\eta'} = 989$  MeV close to the measured masses  $M_\eta^{\text{exp}} = 547.853 \pm 0.0024$  MeV and  $M_{\eta'}^{\text{exp}} = 957.66 \pm 0.24$  MeV [29]. The experiment shows that the vector and excited isoscalar light mesons are almost ideally mixed and therefore can be roughly considered as pure  $q\bar{q}$  and  $s\bar{s}$  states. Indeed we find reasonable agreement of our prediction with experiment in the isoscalar sector.

---

<sup>1</sup> The definition (22) of  $\alpha_s$  can be easily matched with the  $\alpha_s$  used for heavy quarkonia [23] at the scale about  $m_c$ .

TABLE I: Masses of excited light ( $q = u, d$ ) unflavored mesons (in MeV).

$n^{2S+1}L_J$	$J^{PC}$	Theory		Experiment				Theory		Experiment	
		$q\bar{q}$	$I = 1$	mass	$I = 0$	mass	$s\bar{s}$	$I = 0$	mass		
$1^1S_0$	$0^{-+}$	154	$\pi$	139.57				743			
$1^3S_1$	$1^{--}$	776	$\rho$	775.49(34)	$\omega$	782.65(12)	1038	$\varphi$	1019.455(20)		
$1^3P_0$	$0^{++}$	1176	$a_0$	1474(19)	$f_0$	1200-1500	1420	$f_0$	1505(6)		
$1^3P_1$	$1^{++}$	1254	$a_1$	1230(40)	$f_1$	1281.8(6)	1464	$f_1$	1426.4(9)		
$1^3P_2$	$2^{++}$	1317	$a_2$	1318.3(6)	$f_2$	1275.1(12)	1529	$f'_2$	1525(5)		
$1^1P_1$	$1^{+-}$	1258	$b_1$	1229.5(32)	$h_1$	1170(20)	1485	$h_1$	1386(19)		
$2^1S_0$	$0^{-+}$	1292	$\pi$	1300(100)	$\eta$	1294(4)	1536	$\eta$	1476(4)		
$2^3S_1$	$1^{--}$	1486	$\rho$	1465(25)	$\omega$	1400-1450	1698	$\varphi$	1680(20)		
$1^3D_1$	$1^{--}$	1557	$\rho$	1570(70)	$\omega$	1670(30)	1845				
$1^3D_2$	$2^{--}$	1661					1908				
$1^3D_3$	$3^{--}$	1714	$\rho_3$	1688.8(21)	$\omega_3$	1667(4)	1950	$\varphi_3$	1854(7)		
$1^1D_2$	$2^{-+}$	1643	$\pi_2$	1672.4(32)	$\eta_2$	1617(5)	1909	$\eta_2$	1842(8)		
$2^3P_0$	$0^{++}$	1679			$f_0$	1724(7)	1969				
$2^3P_1$	$1^{++}$	1742	$a_1$	1647(22)			2016	$f_1$	1971(15)		
$2^3P_2$	$2^{++}$	1779	$a_2$	1732(16)	$f_2$	1755(10)	2030	$f_2$	2010(70)		
$2^1P_1$	$1^{+-}$	1721					2024				
$3^1S_0$	$0^{-+}$	1788	$\pi$	1816(14)	$\eta$	1756(9)	2085	$\eta$	2103(50)		
$3^3S_1$	$1^{--}$	1921	$\rho$	1909(31)	$\omega$	1960(25)	2119	$\varphi$	2175(15)		
$1^3F_2$	$2^{++}$	1797			$f_2$	1815(12)	2143	$f_2$	2156(11)		
$1^3F_3$	$3^{++}$	1910	$a_3$	1874(105)			2215	$f_3$	2334(25)		
$1^3F_4$	$4^{++}$	2018	$a_4$	2001(10)	$f_4$	2018(11)	2286				
$1^1F_3$	$3^{+-}$	1884					2209	$h_3$	2275(25)		
$2^3D_1$	$1^{--}$	1895	$\rho$	1909(31)			2258	$\omega$	2290(20)		
$2^3D_2$	$2^{--}$	1983	$\rho_2$	1940(40)	$\omega_2$	1975(20)	2323				
$2^3D_3$	$3^{--}$	2066					2338				
$2^1D_2$	$2^{-+}$	1960	$\pi_2$	1974(84)	$\eta_2$	2030(20)	2321				
$3^3P_0$	$0^{++}$	1993	$a_0$	2025(30)	$f_0$	1992(16)	2364	$f_0$	2314(25)		
$3^3P_1$	$1^{++}$	2039	$a_1$	2096(123)			2403				
$3^3P_2$	$2^{++}$	2048	$a_2$	2050(42)	$f_2$	2001(10)	2412	$f_2$	2339(60)		
$3^1P_1$	$1^{+-}$	2007	$b_1$	1960(35)	$h_1$	1965(45)	2398				
$4^1S_0$	$0^{-+}$	2073	$\pi$	2070(35)	$\eta$	2010(50)	2439				
$4^3S_1$	$1^{--}$	2195	$\rho$	2265(40)	$\omega$	2205(30)	2472				
$1^3G_3$	$3^{--}$	2002	$\rho_3$	1982(14)	$\omega_3$	1945(20)	2403				
$1^3G_4$	$4^{--}$	2122	$\rho_4$	2230(25)	$\omega_4$	2250(30)	2481				
$1^3G_5$	$5^{--}$	2264	$\rho_5$	2300(45)	$\omega_5$	2250(70)	2559				
$1^1G_4$	$4^{-+}$	2092					2469				
$3^3D_1$	$1^{--}$	2168	$\rho$	2149(17)			2607				
$3^3D_2$	$2^{--}$	2241	$\rho_2$	2225(35)	$\omega_2$	2195(30)	2667				
$3^3D_3$	$3^{--}$	2309	$\rho_3$	2300(60)	$\omega_3$	2278(28)	2727				
$3^1D_2$	$2^{-+}$	2216	$\pi_2$	2245(60)	$\eta_2$	2248(20)	2662				

TABLE I: (continued)

$n^{2S+1}L_J$	$J^{PC}$	Theory $q\bar{q}$	Experiment				Theory $s\bar{s}$	Experiment	
			$I = 1$	mass	$I = 0$	mass		$I = 0$	mass
$2^3F_2$	$2^{++}$	2091	$a_2$	2100(20)	$f_2$	2141(12)	2514		
$2^3F_3$	$3^{++}$	2191	$a_3$	2070(20)			2585		
$2^3F_4$	$4^{++}$	2284			$f_4$	2320(60)	2657		
$2^1F_3$	$3^{+-}$	2164	$b_3$	2245(50)			2577		
$4^3P_0$	$0^{++}$	2250			$f_0$	2189(13)	2699		
$4^3P_1$	$1^{++}$	2286	$a_1$	2270(50)	$f_1$	2310(60)	2729		
$4^3P_2$	$2^{++}$	2297	$a_2$	2280(30)	$f_2$	2297(28)	2734		
$4^1P_1$	$1^{+-}$	2264	$b_1$	2240(35)	$h_1$	2215(40)	2717		
$2^3G_3$	$3^{--}$	2267	$\rho_3$	2260(20)	$\omega_3$	2255(15)	2743		
$2^3G_4$	$4^{--}$	2375					2819		
$2^3G_5$	$5^{--}$	2472					2894		
$2^1G_4$	$4^{-+}$	2344	$\pi_4$	2250(15)	$\eta_4$	2328(30)	2806		
$5^1S_0$	$0^{-+}$	2385	$\pi$	2360(25)	$\eta$	2320(15)	2749		
$5^3S_1$	$1^{--}$	2491					2782		
$1^3H_4$	$4^{++}$	2234	$a_4$	2237(5)	$f_J$	2231.1(35)	2634		
$1^3H_5$	$5^{++}$	2359					2720		
$1^3H_6$	$6^{++}$	2475	$a_6$	2450(130)	$f_6$	2465(50)	2809		
$1^1H_5$	$5^{+-}$	2328					2706		

The strange meson states ( $L_L$ ) with  $J = L$ , given in Table II, are the mixtures of spin-triplet ( $^3L_L$ ) and spin-singlet ( $^1L_L$ ) states:

$$\begin{aligned} K_J &= K(^1L_L) \cos \varphi + K(^3L_L) \sin \varphi, \\ K'_J &= -K(^1L_L) \sin \varphi + K(^3L_L) \cos \varphi, \quad J = L = 1, 2, 3 \dots \end{aligned} \quad (23)$$

where  $\varphi$  is a mixing angle. Such mixing occurs due to the nondiagonal spin-orbit and tensor terms in Eq. (15). The masses of physical states were obtained by diagonalising the mixing terms. The found values of mixing angle  $\varphi$  are the following:  $1P$   $43.8^\circ$ ,  $2P$   $44.6^\circ$ ,  $3P$   $44.8^\circ$ ,  $1D$   $44.2^\circ$ ,  $2D$   $44.5^\circ$ ,  $1F$   $44.3^\circ$ ,  $1G$   $44.3^\circ$ . These values show that physical  $K_J$  mesons are nearly equal mixtures of the corresponding spin-singlet  $K(^1L_L)$  and spin-triplet  $K(^3L_L)$  states which is in good agreement with the experimental data [29].

The scalar sector presents a special interest due to its complexity and the abundance of experimentally observed light states. We see from Table I that the masses of the lightest  $q\bar{q}$  scalar mesons have values about 1200 MeV. This confirms the conclusion of our recent consideration [21] that light scalar mesons,  $f_0(600)$  ( $\sigma$ ),  $K_0^*(800)$  ( $\kappa$ ),  $f_0(980)$  and  $a_0(980)$ , with masses below 1 GeV should be described as light tetraquarks consisting from scalar diquark and antidiquark. Moreover the predicted masses of the scalar tetraquarks composed from axial-vector diquark and antidiquark [21] have masses in the same range as the lowest  $q\bar{q}$  scalar mesons. Therefore mixing between these states can occur, e.g. due to the instanton-induced mixing terms [31, 32]. The obtained results for the masses indicate that  $a_0(1450)$  should be predominantly a tetraquark state which predicted [21] mass 1480 MeV is within experimental error bars  $M_{a_0(1450)} = 1474 \pm 19$  MeV. The exotic scalar state  $X(1420)$  from the ‘‘Further States’’ Section could be its isotensor partner. On the other hand  $s\bar{q}(1^3P_0)$

TABLE II: Masses of excited strange mesons (in MeV).

$n^{2S+1}L_J$	$J^P$	Theory	Experiment		$n^{2S+1}L_j$	$J^P$	Theory	Experiment	
		$q\bar{s}$	$I = 1/2$	mass			$q\bar{s}$	$I = 1/2$	mass
$1^1S_0$	$0^-$	482	$K$	493.677(16)	$3^1S_0$	$0^-$	2065		
$1^3S_1$	$1^-$	897	$K^*$	891.66(26)	$3^3S_1$	$1^-$	2156		
$1^3P_0$	$0^+$	1362	$K_0$	1425(50)	$2^3D_1$	$1^-$	2063		
$1^3P_2$	$2^+$	1424	$K_2^*$	1425.6(15)	$2^3D_3$	$3^-$	2182		
$1P_1$	$1^+$	1412	$K_1$	1403(7)	$2D_2$	$2^-$	2163	$K_2$	2247(17)
$1P_1$	$1^+$	1294	$K_1$	1272(7)	$2D_2$	$2^-$	2066		
$2^1S_0$	$0^-$	1538			$3^3P_0$	$0^+$	2160		
$2^3S_1$	$1^-$	1675	$K^*$		$3^3P_2$	$2^+$	2206		
$1^3D_1$	$1^-$	1699	$K^*$	1717(27)	$3P_1$	$1^+$	2200		
$1^3D_3$	$3^-$	1789	$K_3^*$	1776(7)	$3P_1$	$1^+$	2164		
$1D_2$	$2^-$	1824	$K_2$	1816(13)	$1^3G_3$	$3^-$	2207		
$1D_2$	$2^-$	1709	$K_2$	1773(8)	$1^3G_5$	$5^-$	2356	$K_5^*$	2382(24)
$2^3P_0$	$0^+$	1791			$1G_4$	$4^-$	2285		
$2^3P_2$	$2^+$	1896			$1G_4$	$4^-$	2255		
$2P_1$	$1^+$	1893			$2^3F_4$	$4^+$	2436		
$2P_1$	$1^+$	1757	$K_1$	1650(50)	$2F_3$	$3^+$	2348	$K_3$	2324(24)
$1^3F_2$	$2^+$	1964	$K_2^*$	1973(26)	$2^3G_5$	$5^-$	2656		
$1^3F_4$	$4^+$	2096	$K_4^*$	2045(9)	$2G_4$	$4^-$	2575	$K_4$	2490(20)
$1F_3$	$3^+$	2080							
$1F_3$	$3^+$	2009							

interpretation is favored for  $K_0^*(1430)$  (see Table II). This picture naturally explains the experimentally observed proximity of masses of the unflavoured  $a_0(1450)$  and  $f_0(1500)$  with the strange  $K_0^*(1430)$ . Therefore one could expect an additional isovector predominantly  $q\bar{q}$  state  $a_0$  with the mass about 1200 MeV, though it was not observed in several experiments.

It was noted long ago that the light meson Regge trajectories are almost linear in  $(J, M^2)$  and  $(n_r, M^2)$  planes.

a) The  $(J, M^2)$  Regge trajectory:

$$J = \alpha M^2 + \alpha_0; \quad (24)$$

b) The  $(n_r, M^2)$  Regge trajectory:

$$n_r \equiv n - 1 = \beta M^2 + \beta_0, \quad (25)$$

where  $\alpha, \beta$  are the slopes and  $\alpha_0, \beta_0$  are intercepts. The relations (24) and (25) arise in most models of quark confinement, but with different values of the slopes. For example, the QCD string with two light quarks at the ends gives the slopes [33]:

$$\alpha = \frac{1}{2\pi\sigma}, \quad \beta = \frac{1}{4\pi\sigma}, \quad (26)$$

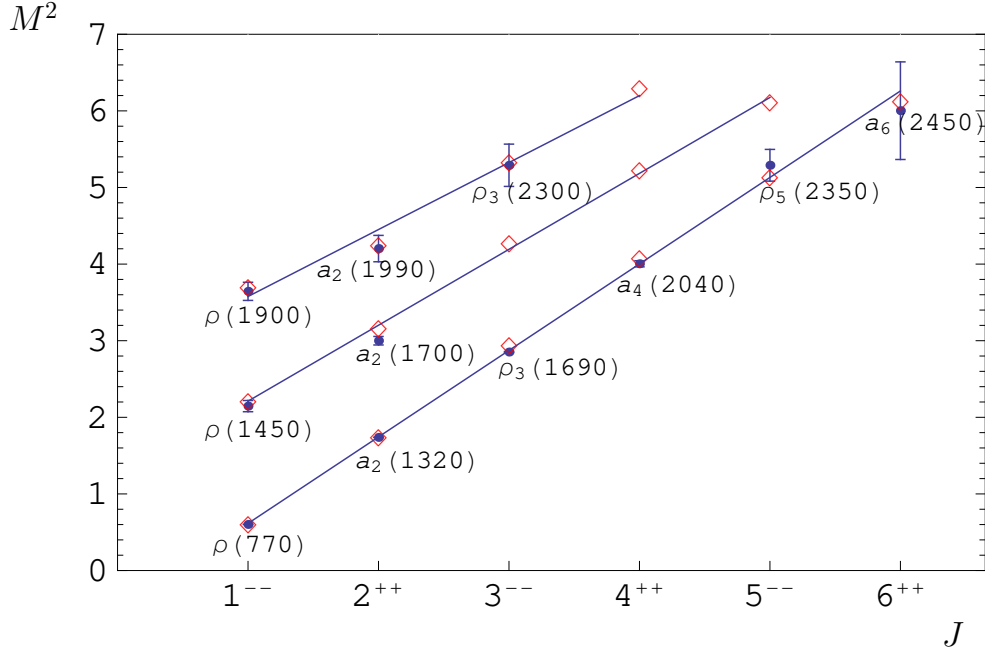


FIG. 1: Parent and daughter  $(J, M^2)$  Regge trajectories for isovector light mesons with natural parity ( $\rho$ ). Diamonds are predicted masses. Available experimental data are given by dots with error bars and particle names.  $M^2$  is in  $\text{GeV}^2$ .

where  $\sigma$  is the string tension which is equal to the slope of the linear confining potential  $A$  in Eq. (10).

On the other hand, the quasiclassical picture for a light meson, described by the massless Salpeter equation with a linear confining potential:

$$(2p + Ar)\psi = M\psi, \quad (27)$$

gives for the Regge slopes [34]

$$\alpha = \frac{1}{8A}, \quad \beta = \frac{1}{4\pi A}, \quad (28)$$

implying that

$$\alpha/\beta = \pi/2. \quad (29)$$

In Figs. 1-5 and Figs. 6-9 we plot the Regge trajectories in the  $(J, M^2)$  plane for mesons with natural ( $P = (-1)^J$ ) and unnatural ( $P = (-1)^{J-1}$ ) parity, respectively. The Regge trajectories in the  $(n_r, M^2)$  plane are presented in Figs. 10-12. The masses calculated in our model are shown by diamonds. Available experimental data are given by dots with error bars and corresponding meson names. Straight lines were obtained by a  $\chi^2$  fit of the calculated values. The fitted slopes and intercepts of the Regge trajectories are given in Tables III and IV. We see that the calculated light meson masses fit nicely to the linear trajectories in both planes. These trajectories are almost parallel and equidistant.

It is important to note that the quality of fitting the  $\pi$  meson Regge trajectories both in  $(J, M^2)$  and  $(n_r, M^2)$  planes is significantly improved if the ground state  $\pi$  is excluded from the fit (the  $\chi^2$  is reduced by more than an order of magnitude and becomes compatible with

TABLE III: Fitted parameters of the  $(J, M^2)$  parent and daughter Regge trajectories for light mesons with natural and unnatural parity ( $q = u, d$ ).

Trajectory	natural parity		unnatural parity	
	$\alpha$ (GeV $^{-2}$ )	$\alpha_0$	$\alpha$ (GeV $^{-2}$ )	$\alpha_0$
$q\bar{q}$	$\rho$		$\pi$	
parent	$0.887 \pm 0.008$	$0.456 \pm 0.018$	$0.828 \pm 0.057^*$	$-0.025 \pm 0.034^*$
daughter 1	$1.009 \pm 0.019$	$-1.232 \pm 0.074$	$1.031 \pm 0.063$	$-1.846 \pm 0.217$
daughter 2	$1.144 \pm 0.113$	$-3.092 \pm 0.540$	$1.171 \pm 0.009$	$-3.737 \pm 0.042$
$q\bar{q}$	$a_0$		$a_1$	
parent	$1.125 \pm 0.035$	$-1.607 \pm 0.104$	$1.014 \pm 0.036$	$-0.658 \pm 0.120$
daughter 1	$1.291 \pm 0.003$	$-3.640 \pm 0.011$	$1.148 \pm 0.012$	$-2.497 \pm 0.050$
daughter 2	$1.336 \pm 0.022$	$-5.300 \pm 0.102$	$1.154 \pm 0.014$	$-3.798 \pm 0.007$
$q\bar{s}$	$K^*$		$K$	
parent	$0.839 \pm 0.004$	$0.318 \pm 0.012$	$0.780 \pm 0.022^\dagger$	$-0.197 \pm 0.036^\dagger$
daughter	$0.942 \pm 0.046$	$-1.532 \pm 0.209$	$0.964 \pm 0.072$	$-2.240 \pm 0.296$
$s\bar{s}$	$\varphi$		$\eta_{s\bar{s}}$	
parent	$0.728 \pm 0.011$	$0.234 \pm 0.034$	$0.715 \pm 0.023$	$-0.444 \pm 0.068$
daughter 1	$0.721 \pm 0.089$	$-1.072 \pm 0.047$	$0.718 \pm 0.032$	$-1.786 \pm 0.157$
daughter 2	$0.684 \pm 0.039$	$-2.047 \pm 0.226$	$0.729 \pm 0.010$	$-3.174 \pm 0.057$

\* fit without  $\pi$ :  $\alpha = (1.053 \pm 0.059)$  GeV $^{-2}$ ,  $\alpha_0 = -0.725 \pm 0.170$

† fit without  $K$ :  $\alpha = (0.846 \pm 0.013)$  GeV $^{-2}$ ,  $\alpha_0 = -0.431 \pm 0.042$

TABLE IV: Fitted parameters of the  $(n_r, M^2)$  Regge trajectories for light mesons.

Meson	$\beta$ (GeV $^{-2}$ )	$\beta_0$	Meson	$\beta$ (GeV $^{-2}$ )	$\beta_0$
$q\bar{q}$			$s\bar{s}$		
$\pi$	$0.679 \pm 0.023^*$	$-0.018 \pm 0.014^*$	$\eta_{s\bar{s}}$	$0.559 \pm 0.009$	$-0.315 \pm 0.026$
$\rho(^3S_1)$	$0.700 \pm 0.023$	$-0.451 \pm 0.060$	$\varphi$	$0.597 \pm 0.009$	$-0.662 \pm 0.031$
$a_0$	$0.830 \pm 0.032$	$-1.214 \pm 0.109$	$f_0$	$0.566 \pm 0.009$	$-1.156 \pm 0.039$
$a_1$	$0.840 \pm 0.037$	$-1.401 \pm 0.134$	$f_1$	$0.561 \pm 0.013$	$-1.224 \pm 0.058$
$b_1$	$0.863 \pm 0.030$	$-1.431 \pm 0.106$	$h_1$	$0.575 \pm 0.015$	$-1.292 \pm 0.066$
$a_2(^3P_2)$	$0.867 \pm 0.036$	$-1.585 \pm 0.134$	$f_2$	$0.581 \pm 0.007$	$-1.370 \pm 0.031$
$\rho(^3D_1)$	$0.894 \pm 0.013$	$-2.182 \pm 0.050$			
$\pi_2$	$0.916 \pm 0.032$	$-2.514 \pm 0.134$			
$\rho_3(^3D_3)$	$0.874 \pm 0.041$	$-2.623 \pm 0.189$			
$a_2(^3F_2)$	$0.891 \pm 0.010$	$-2.881 \pm 0.043$			
$a_3$	$0.890 \pm 0.014$	$-3.254 \pm 0.066$			
$b_3$	$0.906 \pm 0.015$	$-3.225 \pm 0.071$			
$a_4$	$0.899 \pm 0.016$	$-3.672 \pm 0.084$			

\* fit without  $\pi$ :  $\beta = (0.750 \pm 0.032)$  GeV $^{-2}$ ,  $\beta_0 = -0.287 \pm 0.109$

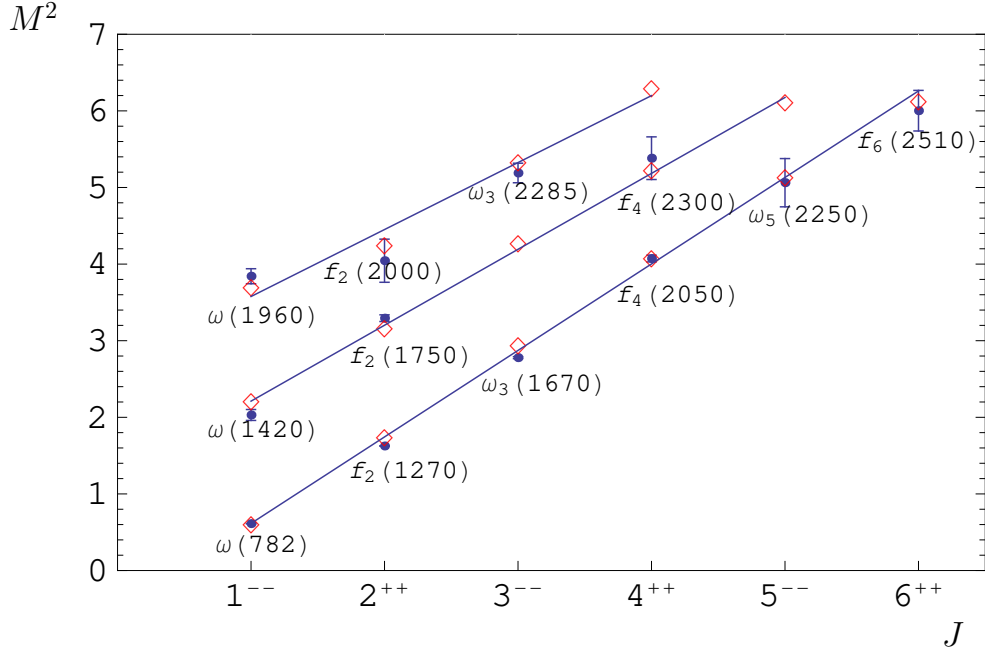


FIG. 2: Same as in Fig. 1 for isoscalar light  $q\bar{q}$  mesons with natural parity ( $\omega$ ).

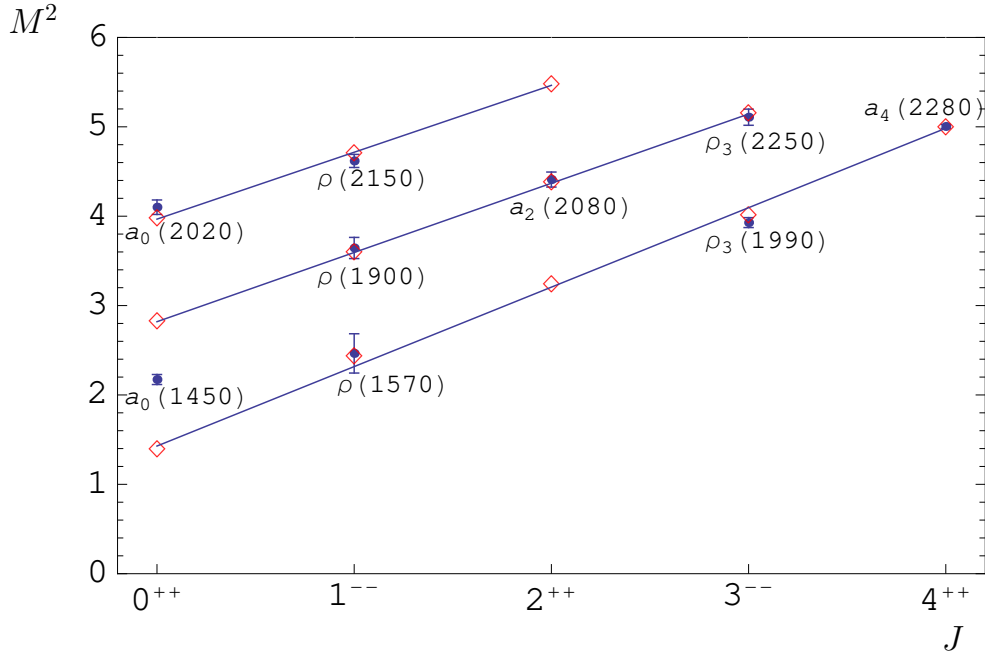


FIG. 3: Same as in Fig. 1 for isovector light  $q\bar{q}$  mesons with natural parity ( $a_0$ ).

the values for other trajectories). In the kaon case omitting the ground state also improves the fit but not so dramatically as for the pion. The corresponding trajectories are shown in Figs. 6, 8 and 10 by dashed lines, the fitted values of the slopes and intercepts are given in the footnotes to Tables III and IV. This indicates the special role of the pion originating from the chiral symmetry breaking.

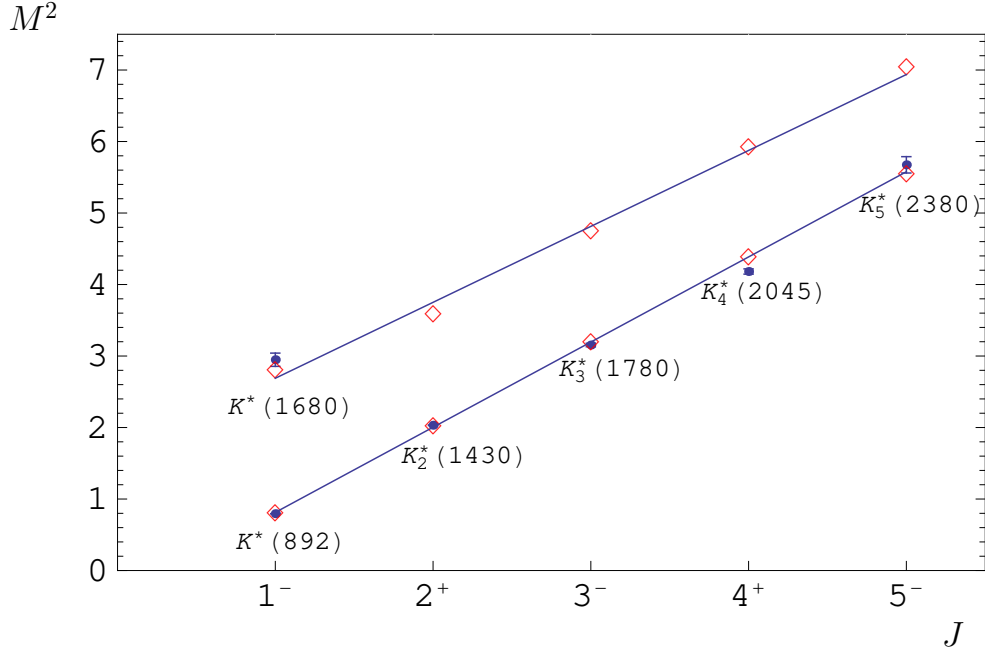


FIG. 4: Same as in Fig. 1 for isodoublet light mesons with natural parity ( $K^*$ ).

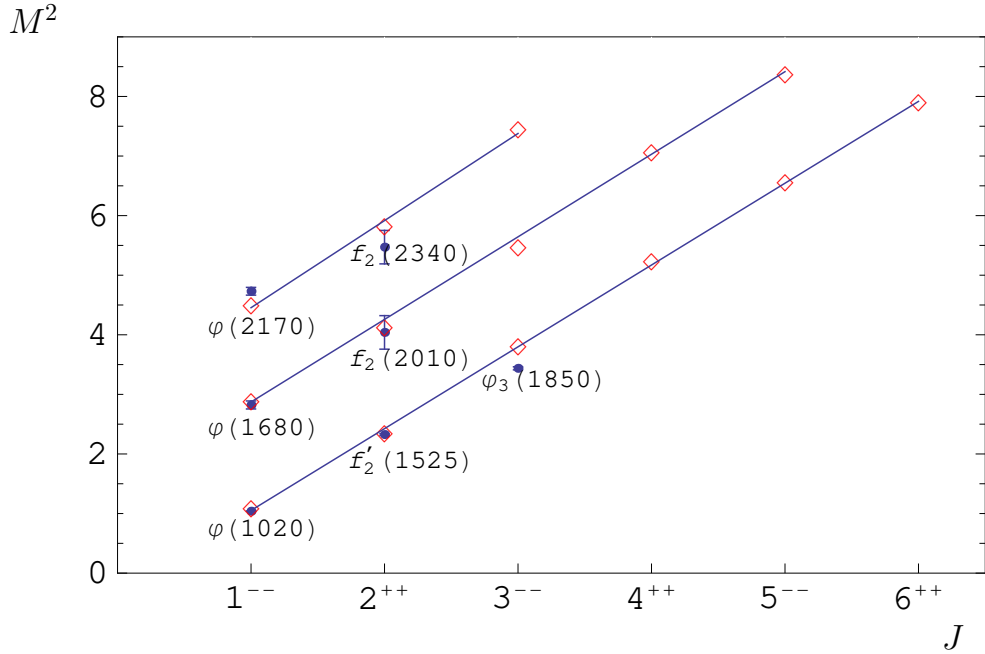


FIG. 5: Same as in Fig. 1 for isoscalar light  $s\bar{s}$  mesons with natural parity ( $\varphi$ ).

It can be seen in Figs. 1 and 3 that  $\rho(1700)$  and  $a_0(1450)$  do not lie on the corresponding Regge trajectories. This further confirms our previous conclusion that  $a_0(1450)$  should be predominantly a tetraquark state and suggests the possible exotic nature of  $\rho(1700)$ .

From the comparison of the slopes in Tables III, IV we see that the  $\alpha$  values are systematically larger than the  $\beta$  ones. The ratio of their mean values is about 1.3 both for the light

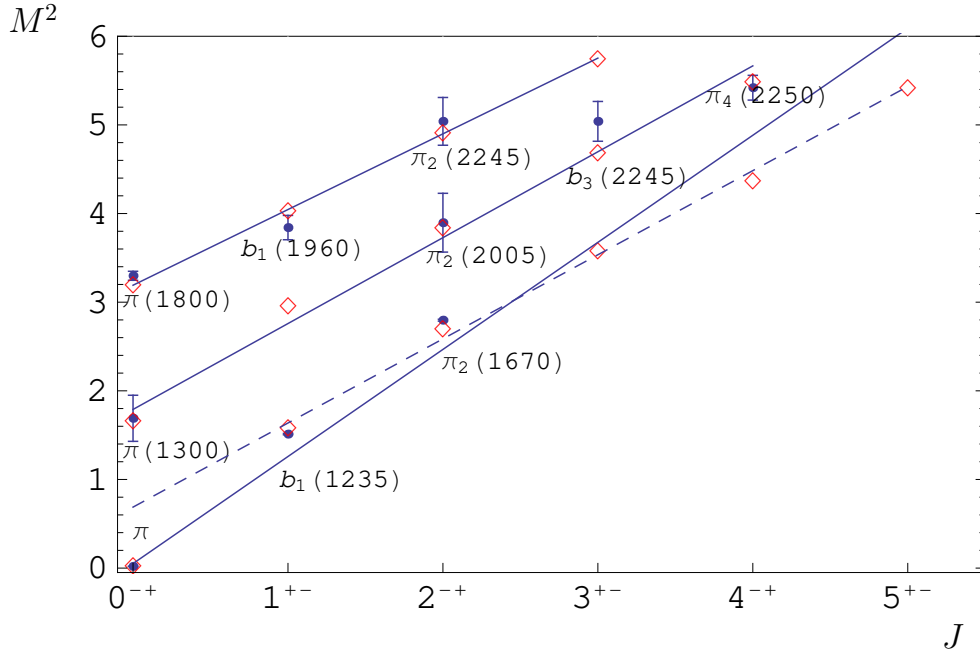


FIG. 6: Same as in Fig. 1 for isovector light mesons with unnatural parity ( $\pi$ ). Dashed line corresponds to the Regge trajectory, fitted without  $\pi$ .

$q\bar{q}$  isovector and  $s\bar{s}$  mesons. Such ratio is lower than predictions of the QCD string model (26) and massless Salpeter equation (29). The mean value of the slope  $\beta \sim 0.85 \text{ GeV}^{-2}$  for isovector mesons is about two times larger than the result of the above mentioned models  $\beta = 1/(4\pi A) \approx 0.44 \text{ GeV}^{-2}$ , for  $A = 0.18 \text{ GeV}^2$  used in our approach.

The assignment of the experimentally observed states to the corresponding Regge trajectories in our model based on their masses and  $J^{PC}$  values (see Figs. 1-12) is slightly different from the previous phenomenological analysis [22, 25] based on the equal values for the slopes  $\alpha$  and  $\beta$ . However the number of states, for which such correspondence is found, is approximately the same. Future experimental data will shed further light on this issue.

## V. CONCLUSIONS

The mass spectra of light quark-antiquark mesons were calculated in the framework of the QCD-motivated relativistic quark model. All considerations were carried out without application of the unjustified nonrelativistic  $v/c$  expansion. Such approach leads to the nonlocal quasipotential of the relativistic quark-antiquark interaction. To make it local, the substitution (11) was used. As a result the relativistic local quasipotential was obtained which depends on the mass of the meson in a complicated nonlinear way. Such dependence allowed us to get masses of the  $\pi$  and  $K$  mesons in agreement with experimental data in the considered model, where the chiral symmetry is explicitly broken by the constituent quark masses. It was found that the lightest scalar ( $1^3P_0$ ) states have masses above 1 GeV. This confirms our previous conclusion [21] that  $f_0(600)$  ( $\sigma$ ),  $K_0^*(800)$  ( $\kappa$ ),  $f_0(980)$  and  $a_0(980)$  could be the diquark-antidiquark tetraquark states. It was found that the calculated masses of light mesons reproduce the linear Regge trajectories both in the  $(J, M^2)$  and  $(n_r, M^2)$  planes. Their slopes and intercepts were determined. The slope of the orbital excitations

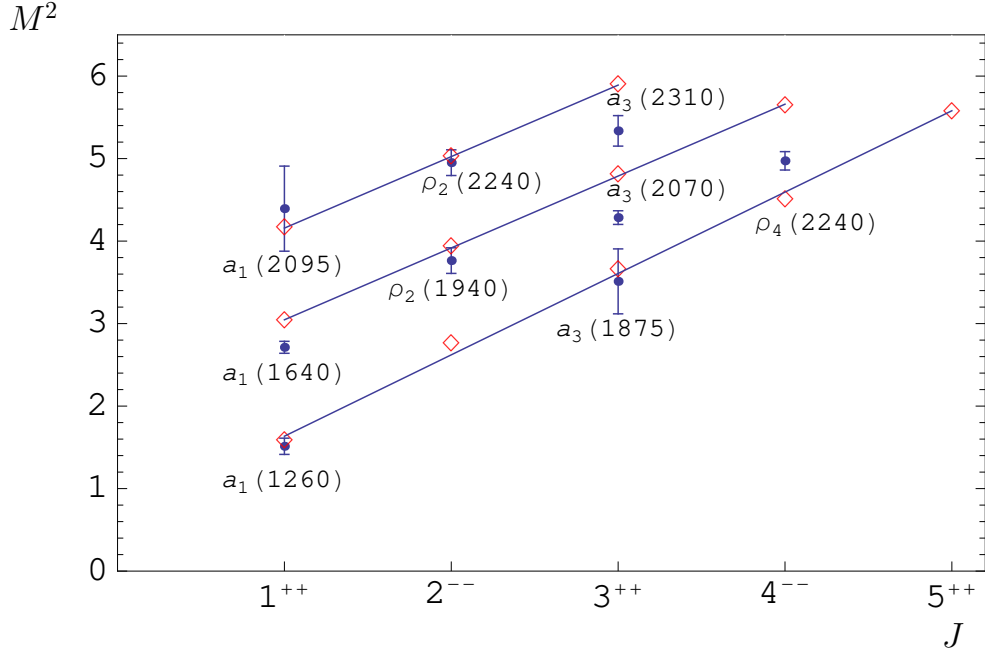


FIG. 7: Same as in Fig. 1 for isovector light  $q\bar{q}$  mesons with unnatural parity ( $a_1$ ).

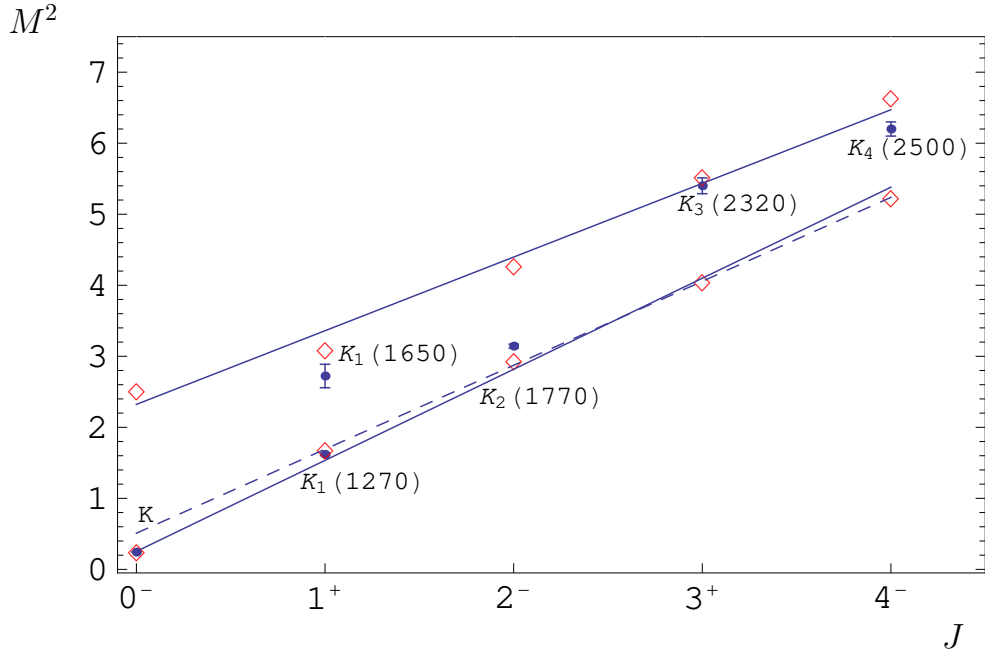


FIG. 8: Same as in Fig. 1 for isodoublet light mesons with unnatural parity ( $K$ ). Dashed line corresponds to the Regge trajectory, fitted without  $K$ .

$\alpha$  was found to be in average 1.3 times larger than the slope of the trajectories of radial excitations  $\beta$ . This value of the ratio  $\alpha/\beta$  is smaller than the predictions based on the spinless Salpeter equation (27) and the QCD string model. The obtained slope  $\beta$  for the isovector light mesons is almost two times higher than the value predicted by the above models. Possible experimental candidates for the states populating the Regge trajectories

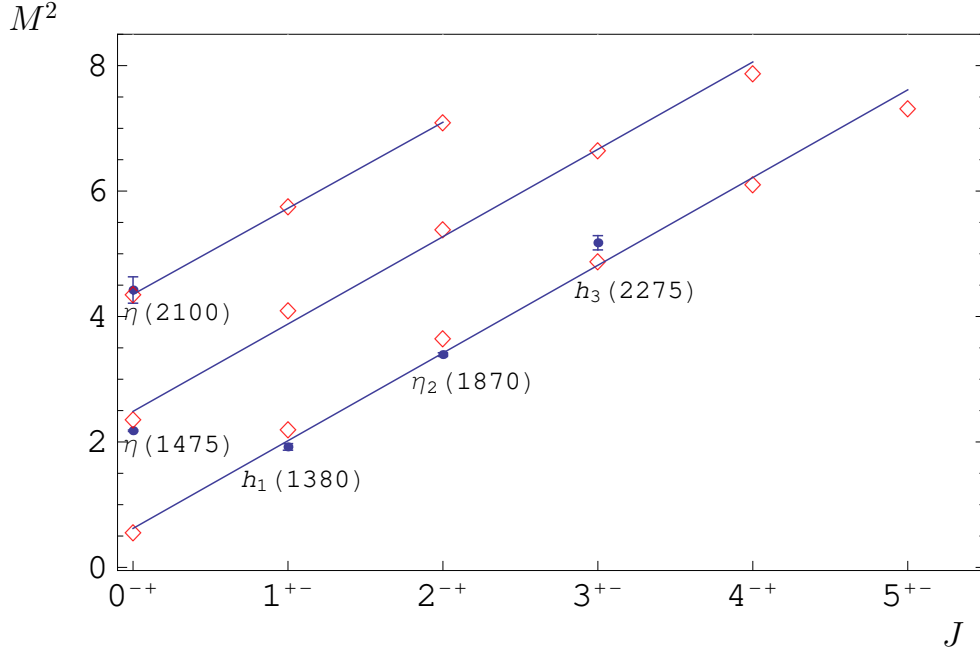


FIG. 9: Same as in Fig. 1 for isoscalar light  $s\bar{s}$  mesons with unnatural parity. The ground state with  $J = 0$  is the mixture of  $\eta$  and  $\eta'$  with pure  $s\bar{s}$  quark content ( $\eta_{s\bar{s}}$ ).

are identified in Figs. 1-12. Predictions for the masses of the missing states are presented in Tables I,II. It is clearly seen that the chiral symmetry is not restored for highly excited states in our model. This should be expected since the Lorentz-scalar part of the confining potential explicitly breaks the chiral symmetry. Our results in some cases differ from the previous phenomenological prescriptions [22, 25]. Future experimental data can help in discriminating between the theoretical predictions.

The authors are grateful to S. Gerasimov, H. Forkel, V. Matveev, V. Savrin, D. Shirkov and A. Vainshtein for support and discussions. This work was supported in part by the Russian Science Support Foundation (V.O.G.) and the Russian Foundation for Basic Research (RFBR), grant No.08-02-00582 (R.N.F. and V.O.G.).

- 
- [1] D. V. Bugg, Phys. Rep. **397**, 257 (2004).
  - [2] A. V. Anisovich *et al.*, Phys. Lett. B **542**, 19 (2002).
  - [3] C. Amsler and N. A. Tornqvist, Phys. Rep. **389**, 61 (2004).
  - [4] E. Klempt and A. Zaitsev, Phys. Rep. **454**, 1 (2007).
  - [5] V. Crede and C. A. Meyer, arXiv:0812.0600 [hep-ex].
  - [6] N. N. Achasov, arXiv:0810.2601 [hep-ph].
  - [7] L. Ya. Glozman, Phys. Rep. **444**, 1 (2007).
  - [8] M. Shifman and A. Vainshtein, Phys. Rev. D **77**, 034002 (2008).
  - [9] S. Godfrey and N. Isgur, Phys. Rev. D **32**, 189 (1985).
  - [10] P. Maris and C.D. Roberts, Int.J. Mod. Phys. E **12**, 297 (2003); P. Maris and P.C. Tandy, Phys. Rev. C **60**, 055214 (1999).

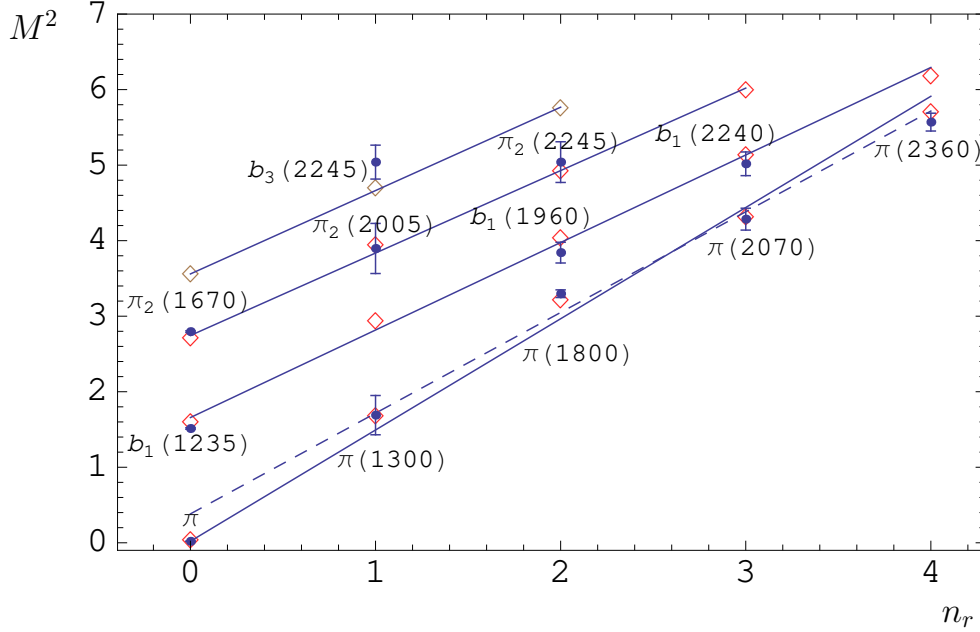


FIG. 10: The  $(n_r, M^2)$  Regge trajectories for spin-singlet isovector mesons  $\pi$ ,  $b_1$ ,  $\pi_2$  and  $b_3$  (from bottom to top). Notations are the same as in Fig. 1. The dashed line corresponds to the Regge trajectory, fitted without  $\pi$ .

- [11] M. Koll, R. Ricken, D. Merten, B. C. Metsch and H. R. Petry, *Eur. Phys. J. A* **9**, 73 (2000).
- [12] M. Baldicchi, A. V. Nesterenko, G. M. Prospero, D. V. Shirkov and C. Simolo, *Phys. Rev. Lett.* **99**, 242001 (2007).
- [13] N. Ligterink and E. S. Swanson, *Phys. Rev. C* **69**, 025204 (2004); F. J. Llanes-Estrada and S. R. Cotanch, *Nucl. Phys. A* **697**, 303 (2002).
- [14] D. Ebert, H. Reinhardt and M.K. Volkov, *Prog. Part. Nucl. Phys.* **33**, 1 (1994); M.K. Volkov, D. Ebert and M. Nagy, *Int. J. Mod. Phys. A* **13**, 5443 (1998); M.K. Volkov and C. Weiss, *Phys. Rev. D* **56**, 221 (1997).
- [15] N.V. Krasnikov and A.A. Pivovarov, *Phys. Lett. B* **112**, 397 (1982); N.V. Krasnikov, A.A. Pivovarov and N.N. Tavkhelidze, *Z. Phys. C* **19**, 301 (1983); A.L. Kataev, hep-ph/9805218.
- [16] A. Ali Khan et al., *Phys. Rev. D* **65**, 054505 (2002).
- [17] H. Forkel, M. Beyer and T. Frederico, *JHEP* **0707**, 077 (2007).
- [18] S. S. Afonin, arXiv:0903.0322 [hep-ph].
- [19] D. Ebert, R. N. Faustov and V. O. Galkin, *Mod. Phys. Lett. A* **20**, 1887 (2005).
- [20] D. Ebert, R. N. Faustov and V. O. Galkin, *Eur. Phys. J. C* **47**, 745 (2006).
- [21] D. Ebert, R. N. Faustov and V. O. Galkin, *Eur. Phys. J. C* **60**, 273 (2009).
- [22] A. V. Anisovich, V. V. Anisovich and A. V. Sarantsev, *Phys. Rev. D* **62**, 051502 (2000); V. V. Anisovich, L. G. Dakhno, M. A. Matveev, V. A. Nikonov and A. V. Sarantsev, *Phys. Atom. Nucl.* **70**, 450 (2007).
- [23] D. Ebert, R.N. Faustov and V.O. Galkin, *Phys. Rev. D* **67**, 014027 (2003).
- [24] D. Ebert, V.O. Galkin and R.N. Faustov, *Phys. Rev. D* **57**, 5663 (1998).
- [25] S. S. Afonin, *Phys. Rev. C* **76**, 015202 (2007)
- [26] H.A. Bethe and E.E. Salpeter, *Quantum Mechanics of One-and Two-Electron Atoms* (Springer-Verlag, Berlin, 1957).

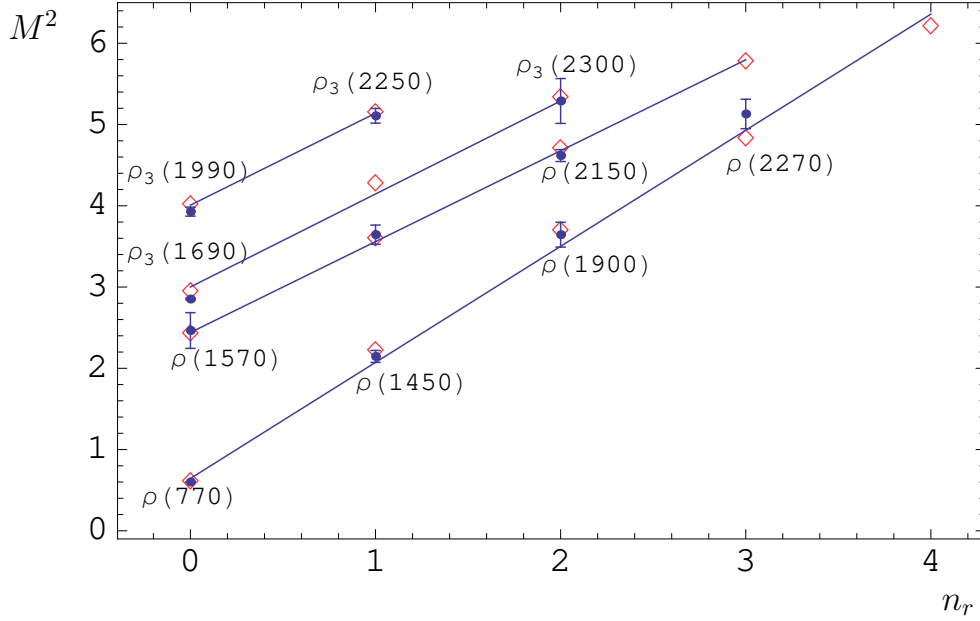


FIG. 11: The  $(n_r, M^2)$  Regge trajectories for spin-triplet isovector mesons  $\rho(^3S_1)$ ,  $\rho(^3D_1)$ ,  $\rho_3(^3D_3)$  and  $\rho_3(^3G_3)$  (from bottom to top). Notations are the same as in Fig. 1.

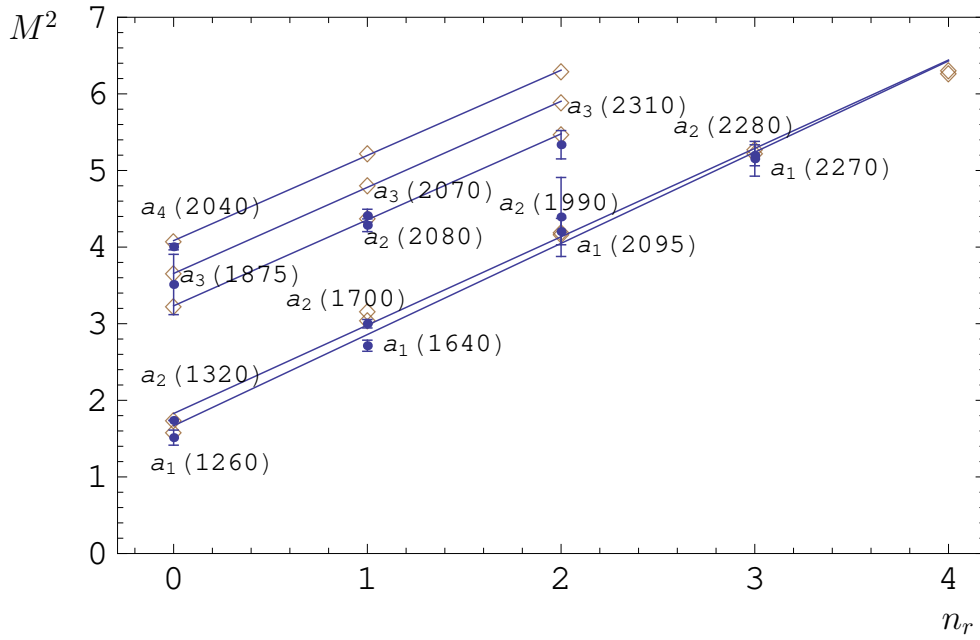


FIG. 12: The  $(n_r, M^2)$  Regge trajectories for spin-triplet isovector mesons  $a_1$ ,  $a_2(^3P_2)$ ,  $a_2(^3F_2)$ ,  $a_3$  and  $a_4(^3F_4)$  (from bottom to top). Notations are the same as in Fig. 1.

- [27] A.M. Badalian, A.I. Veselov and B.L.G. Bakker, Phys. Rev. D **70**, 016007 (2004); Yu.A. Simonov, Phys. Atom. Nucl. **58**, 107 (1995).
- [28] D. Shirkov, arXiv:0807.1404 [hep-ph]; D. V. Shirkov and I. L. Solovtsov, Phys. Rev. Lett. **79**, 1209 (1997).
- [29] C. Amsler *et al.* (Particle Data Group), Phys. Lett. B667, 1 (2008).

- [30] T. Feldmann, P. Kroll and B. Stech, *Phys. Rev. D* **58**, 114006 (1998).
- [31] D. Black, A. H. Fariborz and J. Schechter, *Phys. Rev. D* **61**, 074001 (2000); A. H. Fariborz, R. Jora and J. Schechter, arXiv:0902.2825 [hep-ph].
- [32] G. 't Hooft, G. Isidori, L. Maiani, A. D. Polosa and V. Riquer, *Phys. Lett. B* **662**, 424 (2008)
- [33] Yu. S. Kalashnikova, A. V. Nefediev and Yu. A. Simonov, *Phys. Rev. D* **64**, 014037 (2001); A. Y. Dubin, A. B. Kaidalov and Yu. A. Simonov, *Phys. Lett. B* **323**, 41 (1994); T. J. Allen, C. Goebel, M. G. Olsson and S. Veseli, *Phys. Rev. D* **64**, 094011 (2001).
- [34] P. Bicudo, *Phys. Rev. D* **76**, 094005 (2007).